Published in final edited form as:
Drug Deliv Transl Res. 2012 February 1; 2(1): 45–55. doi:10.1007/s13346-011-0054-y.

Effect of cargo properties on *in situ* forming implant behavior determined by noninvasive ultrasound imaging

Luis Solorio,
Department of Biomedical Engineering, Case Western Reserve University, 10900 Euclid Ave, Cleveland, OH 44106, USA

Alexander M. Olear,
Department of Biomedical Engineering, Case Western Reserve University, 10900 Euclid Ave, Cleveland, OH 44106, USA

Haoyan Zhou,
Department of Biomedical Engineering, Case Western Reserve University, 10900 Euclid Ave, Cleveland, OH 44106, USA

Ashlei C. Beiswenger, and
Department of Biomedical Engineering, Case Western Reserve University, 10900 Euclid Ave, Cleveland, OH 44106, USA

Agata A. Exner
Department of Radiology, Case Center for Imaging Research, Case Western Reserve University, 11100 Euclid Ave, Cleveland, OH 44106, USA

Luis Solorio: luis.solorio@case.edu; Alexander M. Olear: amo29@case.edu; Haoyan Zhou: hxz143@case.edu; Ashlei C. Beiswenger: acb76@case.edu; Agata A. Exner: agata.exner@case.edu

Abstract

Diagnostic ultrasound has been shown to be an effective method for the noninvasive characterization of *in situ* forming implant behavior both in vivo and in vitro through the evaluation of the echogenic signal that forms as a consequence of the polymer phase transition from liquid to solid. The kinetics of this phase transition have a direct effect on drug release and can be altered through factors that change the mass transfer events of the solvent and aqueous environment, including properties of the entrapped active agent. This study examined the effect of payload properties on implant phase inversion, swelling, drug release, and polymer degradation. Poly(DL-lactide-co-gylcolide) implants were loaded with either: sodium fluorescein, bovine serum albumin (BSA), doxorubicin (Dox), or 1′-dioctadecyl-3,3,3′,3′-tetramethylindocarbocyanine perchlorate (DiI). Fluorescein and Dox were released at near equivalent rates throughout the diffusion phase of release but due to differing drug–matrix interactions, Dox-loaded implants released a lower mass of drug during the degradation phase of release. DiI was not readily released, and due to increased depot hydrophobicity, resulted in significantly lower swelling than the other formulations. The initial echogenicity was higher in Dox-loaded implants than those loaded with fluorescein, but after the initial precipitation, phase inversion and drug release occurred at near equivalent rates for both Dox and fluorescein-loaded implants. Nonlinear mathematical fitting was used to correlate drug release and phase inversion, providing a noninvasive method for evaluating implant release (R^2>0.97 for Dox, BSA, and fluorescein; DiI had a correlation coefficient of 0.56).

Luis Solorio and Alexander M. Olear contributed equally to this work.

Keywords

Phase inversion; Ultrasound imaging; In situ forming implant

Introduction

The method by which a therapeutic agent is delivered can drastically alter the concentration profile of the drug in circulation, leading to plasma levels of drug outside the therapeutic window resulting in undesired side effects [1, 2]. The development of drug eluting implant systems provides a method by which drugs can be targeted to the site of action [3–6], plasma concentrations can be maintained for prolonged periods of time [7–13], or local levels of drug can be elevated with limited systemic involvement [4, 8, 9, 14, 15]. Additionally, these systems improve patient compliance as well as protect the drugs from harsh physiological conditions [1, 11, 15]. Although their potential benefits are numerous, oftentimes the fabrication of these devices can be a complicated and expensive process, typically requiring surgical placement [6, 12, 16–20]. One method to overcome these limitations is through the use of a phase sensitive *in situ* forming implant system (ISFI), originally developed by Dunn et al. [21, 22]. These types of implants have been utilized in a number of clinical applications ranging from the delivery of leuprolide acetate for the treatment of prostate cancer (Eligard®, Sonafi-aventis) to the local delivery of anthracyclines for the treatment of periodontal disease (Atridox®, TOLMAR Inc.) [7, 8, 23–25].

ISFIs are manufactured simply by combining a biodegradable polymer, an active drug, and a biocompatible solvent. The resultant solution or suspension can then be injected subcutaneously or directly at the site of action. Once the implant solution comes in contact with the aqueous environment, counter-transport of water into the implant and solvent out results in the formation of a solid drug-eluting polymer depot through a process known as phase inversion [12, 26–28]. The dynamics of this phase inversion process have been shown to correlate with the drug dissolution kinetics, since the rate of liquid–liquid de-mixing is a fundamental factor in the resultant polymer microstructure. In the case of rapidly phase inverting systems, the liquid–liquid de-mixing kinetics typically lead to a porous microstructure with heavily interconnected polymer lean microdomains, which provide paths of high diffusivity through which drug can readily diffuse, resulting in an elevated burst release [26–29]. Therefore, monitoring the phase inversion dynamics provides insight into the underlying implant microstructure and release behavior of the depot [28].

Polymer phase separation has traditionally been monitored using dark ground imaging [26–28, 30]. This method monitors the concentration gradient created by the diffusion of water into the polymer solution. The region of the solution that has undergone a liquid–liquid phase separation is illuminated by the reflection of light. While this technique has been instrumental in determining the fundamental relationship between the rate of phase inversion and drug release, this technique cannot be utilized for *in vivo* applications [18, 20, 27]. Alternatively, electron paramagnetic resonance spectroscopy provides a means for the *in vivo* monitoring of phase inversion. Through the use of a stable lipophilic nitroxyl radical, the magnetic interaction between the free electron and the nuclear spin of nitrogen is utilized to allow the progression of phase inversion from a liquid to solid to be evaluated by monitoring the changes in signal intensity over time. This method is limited in that it requires a free radical nitrogen group to be incorporated in the matrix, which may alter phase inversion dynamics. As a compelling alternative, our group has demonstrated recently that diagnostic ultrasound provides a method to monitor implant behavior in both *in vitro* and *in vivo* settings [20]. The images produced from ultrasound are a result of backscatter generated by differences in the acoustic impedance of the material being imaged (which is a

function of the speed of sound through that material and the material density). Therefore as the polymer precipitates, the resultant change in acoustic impedance gives rise to a backscattered signal that is used to generate an image [19, 20, 31]. Through image analysis techniques, polymer precipitation and implant swelling can be noninvasively monitored.

The behavior of ISF implants can be altered by essentially any factor that changes the nature of the mass transfer dynamics [23, 26, 29, 32–35]. For example, it has been shown that the choice of solvent and polymer can influence the rate of phase inversion and subsequent drug release. Likewise, additives such as Pluronic have also been shown to reduce the burst release of drug due to reduction of the diffusivity of the polymer-lean domains [33, 34] and properties of the drug loaded into the implant may also considerably affect the behavior of the system [35]. In this work, we investigated the role of a variety of drug properties on implant behavior with the help of the ultrasound imaging analysis. Four drugs with different characteristics (Table 1) were evaluated in terms of their effect on implant phase inversion, swelling, release, and polymer degradation. To model the effect of protein loading, bovine serum albumin (BSA), a commonly released model protein, was incorporated into the polymer solution. The lipophilic dye 1, 1′-dioctadecyl-3,3,3′,3′-tetramethylindocarbocyanine perchlorate (DiI, Fig. 1a) was used to evaluate the effects of loading a hydrophobic drug. Finally, to evaluate the effect of a smaller and relatively water-soluble drug, sodium fluorescein (solubility greater than 100 mg/ml, Fig. 1c) and the chemotherapeutic drug doxorubicin (Dox, solubility 10 mg/mL [36], Fig. 1b) were examined. To demonstrate the utility of the ultrasound characterization technique *in vivo*, Dox or fluorescein-loaded implants were injected subcutaneously in Sprague-Dawley rats so that the *in vivo* release, swelling, and phase inversion behavior could also be characterized.

Materials and methods

Materials

Poly(DL-lactic-co-glycolic acid) (PLGA) (50:50 3A, Mw 24,000 Da, inherent viscosity of 0.25 dl/g) was obtained from Lakeshore Biomaterials, Birmingham Al and used as received. *N*-methyl pyrrolidinone (NMP), sodium fluorescein, BSA, and Dox were used as received from Sigma Aldrich (St. Louis, MO). Agarose and phosphate buffered saline (PBS) were received from Fischer Scientific (Waltham, MA). DiI was obtained from Invitrogen (Eugene, OR).

Preparation of polymer formulations

All solutions were prepared using a 39:60:1 mass ratio of PLGA/NMP/drug by first suspending or dissolving the drug in NMP. Polymer was then added to the solution and allowed to incubate overnight in a 37°C shaker table at 90 RPM. Polymer solutions were stored at 4°C and used within 3 days.

In vitro dissolution studies

Drug release profiles were evaluated by injecting 50 μl (roughly 40–50 mg) of polymer–drug solution into 10 ml of 37°C PBS (pH 7.4); implants were then placed in an incubated orbital shaker (37°C at 90 RPM). During the first 8 h, solution was sampled and then replaced with fresh warm PBS at 0, 0.5, 1, 2, 4, 6, and 8 h after implant formation. After the first 24 h, the bath solution was sampled, and then completely removed and replaced by 10 mL of fresh buffer solution daily for 14 days (d). After 14 d, implants were removed from the bath solution and solubilized so that the residual drug mass could be determined. Implants loaded with fluorescein were dissolved in 2 M NaOH. Fluorescein mass was determined by measuring the fluorescence in the solution samples and referenced to a standard curve of known masses on a multimode microplate reader (Tecan Ltd., Infinite 200

series) at excitation/emission wavelengths (Ex/Em) of 485/525 nm. Implants loaded with DiI and Dox were dissolved in 5 ml of NMP. DiI concentration was determined by measuring absorbance on the microplate reader at 549 nm, while Dox concentration was determined using fluorescence with an Ex/Em wavelengths of 470/585 nm. BSA release was determined using a micro-BCA total protein assay kit (Pierce Biotechnology, Rockford, IL), and residual protein mass was determined by degrading the implants in a 0.9 M NaOH solution and then neutralizing the solution with a 0.9 M HCl solution before the residual protein mass was evaluated with the micro-BCA kit. The cumulative drug release was calculated from these measurements and normalized by the actual total initial drug loading at.

In vitro ultrasound imaging

Implants were imaged using ultrasound as previously described [20]. Briefly, a diagnostic ultrasound using a 12-MHz transducer (Aplio XG, Toshiba Medical Systems) was immobilized below an agarose mold so that the implant could be imaged through the *Z*-axis of the implant. Implants were formed by injecting 50 μl of polymer solution into 1 mL of phosphate buffered saline (PBS, pH 7.4), in an agarose phantom containing a 1 ml void. Images were taken immediately after the implant was injected into the PBS bath, as well as 0.5, 1, 2, 4, 6, and 8 h after injection during the first day. After images were taken, the implants were placed in vials containing 10 ml of warm PBS and placed on an incubated orbital shaker. Implants were then imaged once daily for a period of 10 d. Analysis of ultrasound images was performed using a custom MatLab code (MathWorks Inc., Natick, MA), first by selecting the implant shell, then thresholding the image to create a binary image, and finally summing the pixel values to determine the area of the formed polymer shell as well as the total cross-sectional area of the implant [19, 20]. The rate of phase inversion was determined by monitoring the ratio of the polymer shell to the total cross-sectional area, and the change in cross-sectional area over time was used to monitor the implant swelling [19, 20]. Finally, the first 48 h of release and phase inversion were used to evaluate the relationship between burst release and phase inversion. A mathematical fit was performed using the sum of least squares with MatLab. The equation $F(x)=S_0(1-e^{(-\tau x)})+mx$ was used, where X represents the percent of drug release, $F(x)$= percent formation; S_0 =initial polymer precipitation, (%); τ = time delay, $(\frac{1}{\%release})$; and m is the proportionality constant relating the change in drug concentration to the phase inversion, $(\frac{\%}{\%release})$.

Erosion and degradation study

Changes in implant mass with respect to time were monitored by first recording the initial mass of implants formed by injecting 50 μl of polymer solution into 10 ml of warm PBS (pH 7.4), which were then kept in an incubated shaker (37°C at 90 RPM). In order to maintain sink conditions, 1 ml of bath solution was removed daily and replaced with warm, fresh PBS. Implants were removed from the bath solution at 1, 4, 7, 10, 14, 17, and 21 d. Implants were first frozen and then lyophilized for 4 d, and the final implant mass was then recorded.

Changes in the polymer Mw were then evaluated by dissolving the lyophilized implants in tetrahydrofuran, filtered using a 0.45-μm syringe filter, and analyzed using gel permeation chromatography (GPC; Agilent Technologies 1200 Series). The detectors used were refractive index and variable wavelength (Both from Agilent Technologies 1200 Series) and the columns used were two of AM GPC Gel linear/10u and an AM GPC Gel Guard column/ 10u in series (American Polymer Standards Corp). The flow rate of 1 ml/min was used and the results were compared to a polystyrene standard.

Scanning electron microscope imaging and analysis

Implant microstructure was evaluated by first preparing implants by injecting 50 μl of polymer solution into 10 ml of warm PBS. Initially, 5 ml of bath solution was removed and replaced with 5 ml of warm PBS at the conclusion of the 8 h in order to maintain sink conditions. After the first 24 h, 1 ml of bath solution was removed daily and replaced with 1 ml of warm, fresh PBS to keep sink conditions constant. At predetermined time points (3, 7, and 14 days after implantation), the implants were removed from the bath solution, imaged using ultrasound, and then freeze fractured over dry ice. The fractured samples were then lyophilized for 96 h, and then mounted to an aluminum stub and sputter coated with 5 nm of Pd. The coated samples were then imaged using a Quanta 200 3D ESEM with an acceleration voltage of 3.5 kV and a hole size of 10.

In vivo analysis

Animal studies were performed following previously described techniques in accordance with the standards established by the Case Western Reserve University Institutional Animal Care and Use Committee [19, 20]. Briefly, 10 10-week-old male Sprague-Dawley rats (2 rats per time point, with 5 implants per rat) which had an average body weight of 295±15 g (Charles River Laboratories Inc., Wilmington, MA) were anesthetized using 1% isoflurane at a flowing oxygen rate of 1 l/min (EZ150 Isoflurane Vaporizer, EZ Anesthesias™). Implants were formed subcutaneously by injecting 50–70 μl of polymer solution under the dorsal skinflap with an 18-gauge hypodermic needle. Subcutaneous injection was chosen because the current clinical application of a similar formulation (Eligard) is administered in the same manner. The implants were then imaged using the same ultrasound scanner and transducer at 1, 4, 8, 24, and 48 h after implantation. Animals were euthanized at each time point, and the implant was dissected out, followed by dissolution of the implants in order to evaluate the residual drug remaining. Fluorescein and Dox fluorescence was measured using a Tecan 200 series plate reader with Ex/Em wavelengths of 485/525 nm for fluorescein and 470/585 nm for Dox and then referenced to a standard curve.

Statistical analysis

Statistical significance was determined using a one-way analysis of variance (ANOVA, $p<0.05$). A Tukey multicomparison test was used to evaluate differences between groups, with all analysis performed using Minitab (Minitab inc., State College, PA). Unless otherwise noted, all data were reported as mean±standard deviation.

Results

In vitro drug release

ISFIs have characteristic release kinetics consisting of three distinct phases of release: burst (0–24 h), diffusion (between 24 and 216 h), and degradation (216–336 h). During the initial period of release, implants loaded with Dox had the highest overall dissolution of drug followed by fluorescein and BSA, with 27.2±1.8%, 23.2±3.2%, and 21.4±1.4%, respectively (Fig. 2). DiI had a significantly lower burst, releasing only 0.2±.03% during that 24 h period (Fig. 2). The mean mass of drug released per day during the diffusion phase was statistically greater for Dox and fluorescein (3.2±1.1% and 2.7± 1.2%, respectively), than both BSA and DiI (1.0±0.3% and 0.03±0.02%). During the degradation phase, drug dissolution increased relative to the diffusion phase for both fluorescein and DiI (6.5±0.8% and 0.2±0.1%), while decreasing for Dox and BSA (1.5±0.3% and 0.2±0.1%, respectively). Release percentages are summarized in Table 2.

Ultrasound characterization and image validation

Representative gray-scale images of the implants are shown in Fig. 3. Initially, the implants formed a thin shell, and as phase inversion progressed, gray-scale intensity increased as a result of acoustic impedance differences occurring as the polymer precipitated. Implants loaded with fluorescein and DiI formed pores near the center of the implants which increased in diameter over time (Fig. 3a, b). For implants loaded with BSA and Dox, these pores were present initially, but did not expand over time (Fig. 3c, d). Image validation was performed by comparing ultrasound images to pictures of cryosectioned implants and SEM micrograms. These same implants were compared with 7 d images at a higher magnification. Hyperechoic regions were generated as a result of the heterogeneous microstructures formed during phase inversion, with isoechoic regions corresponding to polymer lean domains within the implant microstructure (Fig. 4).

Phase inversion—Initially, polymer precipitation occurred rapidly with only negligible changes in echogenicity occurring after 4 h, with DiI-loaded implants showing the greatest rate of precipitation, transitioning from an initial phase inverted area occupying 29.3±6.0% to a plateau value of 78.2±6.1% (Fig. 5a, d). Dox and BSA-loaded implants both had an increased initial echogenic signal that occupied a larger portion of the cross-sectional area (50.9±7.1% and 58.8±6.0%) and reached a statistically equivalent plateau 4 h after implantation to the DiI-loaded implants (Fig. 5a, d). Conversely, fluorescein-loaded implants had an initial precipitation area of 22.0±11.0% initially, and reached a plateau of 58.7±13.2%, showing a similar rate of change to both BSA and Dox-loaded implants (Fig. 5a, d).

After 24 h the implants continued to precipitate, but more gradually, with DiI-loaded implants reaching a maximum precipitated area 48 h after implantation, fluorescein-loaded depots 96 h after implantation, Dox and BSA-loaded implants reaching maximums after 144 h (84.0±5.6%, 88.8±5.8%, 92.7±2.0%, and 95.1±4.1%). The polymer area remained constant for 3 d after phase inversion was complete. For implants loaded with DiI, fluorescein, and Dox, phase inversion was followed by a decrease in precipitated area during the duration of the study, and to a much smaller extent with BSA-loaded implants (Fig. 5a).

Implant swelling—Implants loaded with DiI initially shrank, losing 15.0±7.4% of the original cross-sectional area, with no change observed until after 8 h in solution (Fig. 5b). After 8 h, the implants began to swell and approached the original cross-sectional area after 24 h. Swelling continued until a maximum of 31.2±9.8% greater than the original cross-sectional area was reached after 144 h in buffer. An initial decrease in implant cross-sectional area was also observed with both Dox and fluorescein-loaded implants (14.6±2.5% and 4.8±5.3%, respectively). Depots loaded with Dox began to approach the original size after 4 h in buffer, while the fluorescein-loaded implants only took 1 h. Both implants loaded with Dox and those loaded with fluorescein continued to swell, with Dox-loaded implants increasing an additional 70.7±15.8% relative to the original cross-sectional area after 120 h and fluorescein-loaded implants increasing 75.6±23.5% after 168 h (Fig. 5b). BSA-loaded implants did not shrink initially, but after an initial period of expansion increasing in size by 11.85±9.3% after 1 h and only negligible changes were observed over the course of next 24 h. After 24 h in solution, the implants began to swell, with area increasing an additional 66.7±10% relative to the original cross-sectional area after 120 h in buffer (Fig. 5b).

Correlation of phase inversion to drug release—A nonlinear relationship was developed correlating the phase inversion to the burst phase of drug release (Fig. 5c). The value S_0 was used to evaluate the initial echogenicity of the implants. Fluorescein had the

lowest S_0 value, followed by Dox, then DiI, and finally BSA (Table 3). The τ value was added to account for the transition to linearity, with DiI and Dox each having τ values greater than 1, indicating a rapid transition into the linear region (Table 3). Finally, the slope was used to evaluate the sensitivity in the linear region.

Erosion and degradation

Initially as a result of NMP loss, mass loss was above 40% for all implant formulations, with no statistical difference between the implants for the first 10 days. After 10 days, implants loaded with DiI and those loaded with fluorescein began to show increased mass loss relative to those implants loaded with Dox or BSA (28.4±2.7%, 29.9±3.3%, 35.3± 1.5%, 34.7±1.4%, respectively; Fig. 6a). Changes in the weight average Mw showed that implants loaded with fluorescein had an initially elevated level of polymer degradation, with the mean Mw reduced by 39.7±12.2% after only 1 day (Fig. 6b). Implants loaded with either Dox or BSA showed reduced degradation relative to the implants loaded with either DiI or fluorescein after 1 week in solution, but after 14 days all implant formulations had undergone a similar level of hydrolysis (Fig. 6b).

Implant microstructure analysis

Comparison of the microstructure that forms as a result of the phase inversion dynamics shows that implants loaded with Dox, fluorescein, and BSA all have a similar cell like microstructure with highly interconnected porous interior (Fig. 7a–d). Conversely, while macroporous structures were formed in the DiI-loaded implants, they appear to be less interconnected with large regions of polymer separating the polymer-lean domains (Fig. 7b). After 7 days in buffer, porosity appears to increase for the fluorescein-loaded implants (Fig. 7e). For the BSA-loaded implants and the Dox-loaded implants the porosity appeared to increase, but the increase in pore size was not as substantial as what was observed in fluorescein-loaded implants (Fig. 7g, h). Implants loaded with DiI showed a less defined structure after 7 days in buffer (Fig. 7f).

In vivo characterization

Polymer precipitation rapidly reached a plateau within the first hour of implantation, and no significant changes were observed over the course of the next 48 h (Fig. 8). No significant difference in phase inversion was observed between implants loaded with Dox or those loaded with fluorescein. Dox dissolution was significantly higher *in vivo* than *in vitro. In vivo*, 42.8% of the drug was lost 1 h after implantation, but release slowed after 1 h, with 58.5% of drug released after 24 h. After 24 h, there was a second burst of release, with 73.4% of the drug lost after 48 h. Release of fluorescein was similar to that of Dox, but fluorescein had a slightly lower initial burst of drug, losing only 28.7% 1 h after implantation, but increased to 47.5% after 8 h. A second burst was observed with 68.3% of fluorescein lost after 24 h and 73.5% after 48 h. Implants loaded with Dox decreased in cross-sectional area for the first 24 h, but showed a modest increase after 48 h. Implants loaded with fluorescein showed a decrease in size over the first 8 h, but swelling was observed after 24 h (Fig. 9).

Discussion

Ultrasound characterization is a noninvasive means by which implants can be evaluated nondestructively in a number of different environments, providing real-time images of polymer precipitation. This nondestructive characterization technique can not only be used to evaluate the effect of injection site on implant behavior, but also how the host responds to the implant [19, 20]. Previous studies have focused on the effect of environment on phase inversion and swelling using a single mock drug, fluorescein [19, 20]. The focus of this

study was to evaluate how various drug properties alter the phase inversion dynamics, swelling, and release properties of the implants. Evaluation of the implant phase inversion showed that polymer precipitation occurred in two steps; first the formation of the polymer shell, which occurred within the first 4 h. Then a slower transition which occurred over the time scale of days, as the implant interior slowly transitioned into a stable matrix. The outer shells of the implants were highly echogenic, with a distinctly different microstructure from the interior domain (Fig. 4). In the case of implants loaded with DiI or fluorescein, a pore formed in the implant center after the implants phase inverted, which gradually increased in size over time. Pore formation also occurred with BSA and Dox-loaded implants, but the pore did not increase in diameter over time. We hypothesize that the pore is initially a result of entropically driven phase separation, and increases in size due to the polymer degradation, which was slower for both BSA and Dox-loaded implants. Additionally, fluorescein, BSA and Dox resulted in a similar microstructure due to their comparable rates of phase inversion. DiI showed a significantly different microstructure, with large macrovoids due to the drug's insolubility in water consequently affecting the implant's phase inversion dynamics. Drug hydrophobicity was a significant factor altering the implant swelling. The implants loaded with the hydrophobic dye DiI showed an initial reduction in cross-sectional area. This indicates that the influx of water into the implant was lower than the efflux of solvent from the implant.

When comparing the burst release to phase inversion, a mathematical relationship was developed to account for the initial echogenicity of the precipitating polymer, providing a means by which the drug release could be approximated noninvasively. While implants loaded with Dox had a higher initial precipitation, the phase inversion and drug release occurred at near equivalent rates. Interestingly the relationship between phase inversion and drug release for implants loaded with BSA was negative, which we hypothesize to be a result of the crystallized BSA dissolving as water diffused into the matrix during the phase inversion process. While the correlation coefficient was above 0.97 for implants loaded with Dox, fluorescein, or BSA, this relationship did not hold for DiI-loaded implants. The poor correlation is suspected to be a result of the low mass of drug that is released by these implants. While a relationship exists between polymer precipitation and burst release, because of the rapidly reached plateau in phase inversion and elevated levels of drug release, the sensitivity was lower than what was observed *in vitro*.

When the erosion and degradation behavior of the implants was evaluated, rapid mass loss was observed for both DiI and fluorescein-loaded implants, but the rate of erosion was slower for the implants loaded with Dox and BSA. While this result was not anticipated, it has been observed that the internal environment of PLGA microparticles is acidic with a pH ranging from 2 to 5 [37]. It has also been reported that BSA has a maximum buffering capacity of pH 3.5 [38], indicating that BSA may be acting as a buffer and delaying polymer degradation. In the case of Dox-loaded implants, we speculate that as a consequence of the low pH, Dox becomes positively charged. Over time as buffer diffuses into the implants and the acidic byproducts diffuse out, internal pH increases closer to 5 [37] (above the p*K*a of the polymer [39]) resulting in a net negative charge state within the matrix, leading to the formation of an ionic complex that retards both the mass loss of drug and polymer degradation. The potential for ionic complexation is not limited to Dox. In addition to the buffering capacity of BSA at low pH, the isoelectric point is between pH 4.7 and 4.9 [40], which indicates that the protein will be in a cationic state when loaded in the polymer matrix. The resultant electrostatic interactions may be an additional contributing factor altering the release and degradation profile of BSA-loaded implants. As neither DiI nor fluorescein would interact with the matrix, release is elevated as the polymer degrades.

Release *in vivo* has been shown to be elevated relative to the release observed *in vitro* [19, 20, 41]. Interestingly, beyond the high initial burst, secondary burst releases occurred in accordance with observed increases in polymer cross-sectional area (Fig. 9). The resultant changes in implant geometry may enhance drug release in two ways, by first increasing the surface area for drug diffusion and secondly by introducing convective forces within the implant elevating drug release.

The noninvasive technique utilized in this study was able to successfully quantify the relative longitudinal implant behavior *in vitro* and *in vivo* and offer some insights into the complex relationship between drug properties and their effects on implant formation and erosion. Nonetheless, some limitations remain. One point of concern is the effect of drug itself on the ultrasound signal. In the majority of cases, since ultrasound characterizes phase inversion through monitoring changes in polymer matrix echogenicity, the addition of drug should not affect the characterization process. Indeed, in the case of drugs that readily dissolve in the polymer solution, no interference was observed. However, in the case of drugs with low solubility in the polymer solution, there was an elevated initial echogenic signal. We hypothesize that this elevated signal is a result of the non-dissolved agent causing an acoustic impedance mismatch between the liquid polymer and crystallized drug, leading to hyperechoic regions within the liquid interior of the implant. Since BSA is not soluble in NMP, the resultant polymer suspension led to the hyperechoic domains. While Dox is soluble in NMP, elevated concentrations of the drug have been show to result in the formation of aggregates [2, 42, 43], which would then act as a scattering agent within the liquid interior of the implant. Despite the initial elevated background signal, in all cases relative polymer precipitation could still be observed and successfully quantified.

Conclusion

Advances in medical imaging have led to the development of tools for accurate placement of devices in the body as well as methods for monitoring treatment efficacy. In the field of drug delivery, these tools can also be used in order to better understand how a delivery system is behaving in the body, so that deviations in device behavior can be better understood. This study demonstrated that ultrasound imaging could be used to monitor implant behavior regardless of the drug loading both *in vitro* and *in vivo*. The ability to noninvasively monitor the behavior of implants in their unperturbed environment, whether *in vitro* or *in vivo* provides a means by which the interactions between the drug, the matrix, and the injection site can be more fully understood. In this study a relationship was established between phase inversion and drug release which provides a means by which burst release of implants can be approximated. Additionally, alternative imaging techniques, such as MRI, could prove useful in further investigation of implant behavior, providing insight into other characteristics such as solvent exchange. As the image-guided drug delivery field evolves, these techniques could in the near future be utilized in the clinic to better understand and subsequently improve *in situ* forming implant performance and hopefully broaden their application scope.

Acknowledgments

This work was supported by NIH grant R01CA118399 to AAE and T32EB007509-01 to LS. The authors would like to thank Casey Johnson and Divya Sundarapandiyan for the technical assistance in this project.

References

1. Lewis AL, Illum L. Formulation strategies for sustained release of proteins. Ther Deliv. 2010; 1(3): 457–79.

2. Manocha, B.; Margaritis, A. Journal of Nanomaterials: Controlled release of doxorubicin from doxorubicin/gamma-polyglutamic acid ionic complex. 2010.
3. Arifin DY, Lee KY, Wang CH. Chemotherapeutic drug transport to brain tumor. J Control Release. 2009; 137(3):203–10. [PubMed: 19376172]
4. Jain RA, Rhodes CT, Railkar AM, Malick AW, Shah NH. Controlled release of drugs from injectable in situ formed biodegradable PLGA microspheres: effect of various formulation variables. Eur J Pharm Biopharm. 2000; 50(2):257–62. [PubMed: 10962236]
5. Krupka TM, Weinberg BD, Ziats NP, Haaga JR, Exner AA. Injectable polymer depot combined with radiofrequency ablation for treatment of experimental carcinoma in rat. Invest Radiol. 2006; 41(12):890–7. [PubMed: 17099428]
6. Saltzman WM, Fung LK. Polymeric implants for cancer chemotherapy. Adv Drug Deliv Rev. 1997; 26(2–3):209–30. [PubMed: 10837544]
7. Al-Tahami K, Oak M, Singh J. Controlled delivery of basal insulin from phase-sensitive polymeric systems after subcutaneous administration: in vitro release, stability, biocompatibility, in vivo absorption, and bioactivity of insulin. J Pharm Sci. 2011; 100(6):2161–2171. [PubMed: 21491440]
8. Dunn RL, Garrett S. The drug delivery and biomaterial attributes of the ATRIGEL technology in the treatment of periodontal disease. Expert Opin Investig Drugs. 1998; 7(9):1483–91.
9. Hatefi A, Amsden B. Biodegradable injectable in situ forming drug delivery systems. J Control Release. 2002; 80(1–3):9–28. [PubMed: 11943384]
10. Kranz H, Yilmaz E, Brazeau GA, Bodmeier R. In vitro and in vivo drug release from a novel in situ forming drug delivery system. Pharm Res. 2008; 25(6):1347–54. [PubMed: 17968634]
11. Packhaeuser CB, Schnieders J, Oster CG, Kissel T. In situ forming parenteral drug delivery systems: an overview. Eur J Pharm Bio-pharm. 2004; 58(2):445–55.
12. Ravivarapu HB, Moyer KL, Dunn RL. Sustained suppression of pituitary–gonadal axis with an injectable, in situ forming implant of leuprolide acetate. J Pharm Sci. 2000; 89(6):732–41. [PubMed: 10824131]
13. Singh S, Singh J. Phase-sensitive polymer-based controlled delivery systems of leuprolide acetate: in vitro release, biocompatibility, and in vivo absorption in rabbits. Int J Pharm. 2007; 328(1):42–8. [PubMed: 16959451]
14. Eliaz RE, Kost J. Characterization of a polymeric PLGA-injectable implant delivery system for the controlled release of proteins. J Biomed Mater Res. 2000; 50(3):388–96. [PubMed: 10737881]
15. Eliaz RE, Wallach D, Kost J. Delivery of soluble tumor necrosis factor receptor from in-situ forming PLGA implants: in-vivo. Pharm Res. 2000; 17(12):1546–50. [PubMed: 11303966]
16. Exner AA, Saidel GM. Drug-eluting polymer implants in cancer therapy. Expert Opin Drug Deliv. 2008; 5(7):775–88. [PubMed: 18590462]
17. Kempe S, Metz H, Mader K. Do in situ forming PLG/NMP implants behave similar in vitro and in vivo? A non-invasive and quantitative EPR investigation on the mechanisms of the implant formation process. J Control Release. 2008; 130(3):220–5. [PubMed: 18611421]
18. Kempe S, Metz H, Pereira PGC, Mader K. Non-invasive in vivo evaluation of in situ forming PLGA implants by benchtop magnetic resonance imaging (BT-MRI) and EPR spectroscopy. Eur J Pharm Biopharm. 2010; 74(1):102–8. [PubMed: 19545625]
19. Patel RB, Solorio L, Wu HP, Krupka T, Exner AA. Effect of injection site on in situ implant formation and drug release in vivo. J Control Release. 2010; 147(3):350–8. [PubMed: 20728486]
20. Solorio L, Babin BM, Patel RB, Mach J, Azar N, Exner AA. Noninvasive characterization of in situ forming implants using diagnostic ultrasound. J Control Release. 2010; 143(2):183–90. [PubMed: 20060859]
21. Biodegradable in situ forming implants and methods of producing the same. U.S: 1990.
22. Polymeric compositions useful as controlled release implants. U.S: 1997.
23. Brodbeck KJ, Pushpala S, McHugh AJ. Sustained release of human growth hormone from PLGA solution depots. Pharm Res. 1999; 16(12):1825–9. [PubMed: 10644069]
24. Gad HA, El-Nabarawi MA, El-Hady SSA. Formulation and evaluation of PLA and PLGA in situ implants containing secnidazole and/or doxycycline for treatment of periodontitis. AAPS PharmSciTech. 2008; 9(3):878–84.

25. Ravivarapu HB, Moyer KL, Dunn RL. Sustained activity and release of leuprolide acetate from an in situ forming polymeric implant. AAPS PharmSciTech. 2000; 1(1):E1. [PubMed: 14727850]
26. Brodbeck KJ, DesNoyer JR, McHugh AJ. Phase inversion dynamics of PLGA solutions related to drug delivery—Part II. The role of solution thermodynamics and bath-side mass transfer. Journal of Controlled Release. 1999; 62(3):333–44. [PubMed: 10528071]
27. Graham PD, Brodbeck KJ, McHugh AJ. Phase inversion dynamics of PLGA solutions related to drug delivery. J Control Release. 1999; 58(2):233–45. [PubMed: 10053196]
28. McHugh AJ, Graham PD, Brodbeck KJ. Phase inversion dynamics of PLGA solutions related to drug delivery. Biomedical Materials-Drug Delivery, Implants and Tissue Engineering. 1999; 550:41–6.
29. DesNoyer JR, McHugh AJ. Role of crystallization in the phase inversion dynamics and protein release kinetics of injectable drug delivery systems. J Control Release. 2001; 70(3):285–94. [PubMed: 11182199]
30. Mchugh AJ, Miller DC. The dynamics of diffusion and gel growth during nonsolvent-induced phase inversion of polyethersulfone. J Membr Sci. 1995; 105(1–2):121–36.
31. Solorio L, Patel RB, Wu H, Krupka T, Exner AA. Advances in image-guided intratumoral drug delivery techniques. Ther Deliv. 2010; 1(2):307–22.
32. Bakhshi R, Vasheghani-Farahani E, Mobedi H, Jamshidi A, Khakpour M. The effect of additives on naltrexone hydrochloride release and solvent removal rate from an injectable in situ forming PLGA implant. Polym Adv Technol. 2006; 17(5):354–9.
33. DesNoyer JR, McHugh AJ. The effect of Pluronic on the protein release kinetics of an injectable drug delivery system. J Control Release. 2003; 86(1):15–24. [PubMed: 12490369]
34. Patel RB, Carlson AN, Solorio L, Exner AA. Characterization of formulation parameters affecting low molecular weight drug release from in situ forming drug delivery systems. J Biomed Mater Res A. 2010; 94A(2):476–84. [PubMed: 20186771]
35. Tang Y, Singh J. Controlled delivery of aspirin: effect of aspirin on polymer degradation and in vitro release from PLGA based phase sensitive systems. Int J Pharm. 2008; 357(1–2):119–25. [PubMed: 18329202]
36. Zhang HT, Li F, Yi J, Gu CH, Fan L, Qiao YB, et al. Folate-decorated maleilated pullulan-doxorubicin conjugate for active tumor-targeted drug delivery (vol 42, pg 517, 2011). European Journal of Pharmaceutical Sciences. 2011; 43(5):409.
37. Ding AG, Schwendeman SP. Acidic microclimate pH distribution in PLGA microspheres monitored by confocal laser scanning microscopy. Pharm Res. 2008; 25(9):2041–52. [PubMed: 18622692]
38. Curvale RA. Buffer capacity of bovine serum albumin (BSA). J Argent Chem Soc. 2009; 97(1): 174–80.
39. Zolnik BS, Burgess DJ. Effect of acidic pH on PLGA microsphere degradation and release. J Control Release. 2007; 122(3):338–44. [PubMed: 17644208]
40. Righetti PG, Caravaggio T. Isoelectric points and molecular-weights of proteins: A table. J Chromatogr. 1976; 127(1):1–28. [PubMed: 6485]
41. Liu QF, Zhang H, Zhou GC, Xie SB, Zou H, Yu YA, et al. In vitro and in vivo study of thymosin alpha1 biodegradable in situ forming poly(lactide-co-glycolide) implants. Int J Pharm. 2010; 397(1–2):122–9. [PubMed: 20650309]
42. Abraham SA, Edwards K, Karlsson G, MacIntosh S, Mayer LD, McKenzie C, et al. Formation of transition metall-doxorubicin complexes inside liposomes. Biochimica Et Biophysica Acta-Biomembranes. 2002; 1565(1):41–54.
43. Deng W, Li JA, Yao P, He F, Huang C. Green preparation process, characterization and antitumor effects of doxorubicin-bsa-dextran nanoparticles. Macromol Biosci. 2010; 10(10):1224–34. [PubMed: 20602420]
44. Lavis LD, Rutkoski TJ, Raines RT. Tuning the pK(a) of fluorescein to optimize binding assays. Anal Chem. 2007; 79(17):6775–82. [PubMed: 17672523]

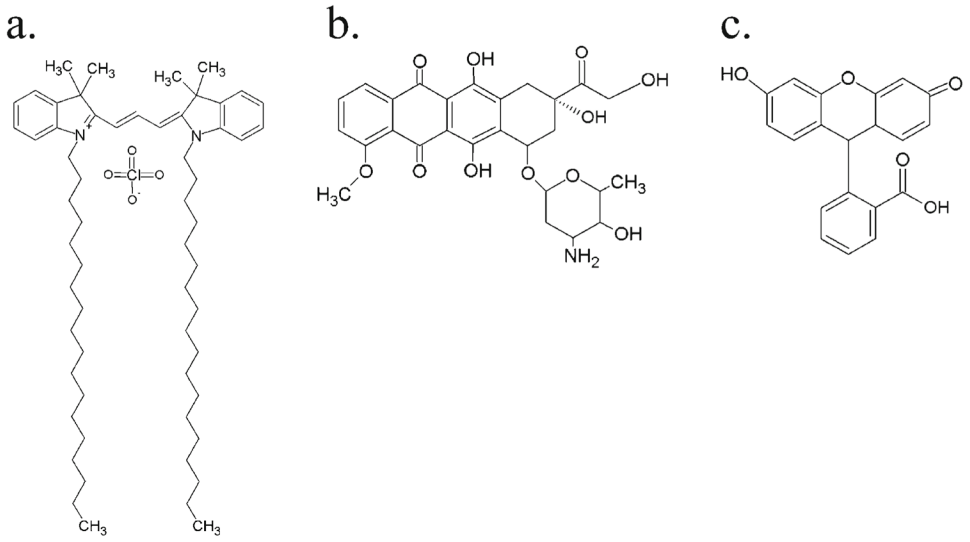

Fig. 1.

The chemical structures of the drugs used in this study: (**a**) DiI, (**b**) Dox, (**c**) Fluorescein

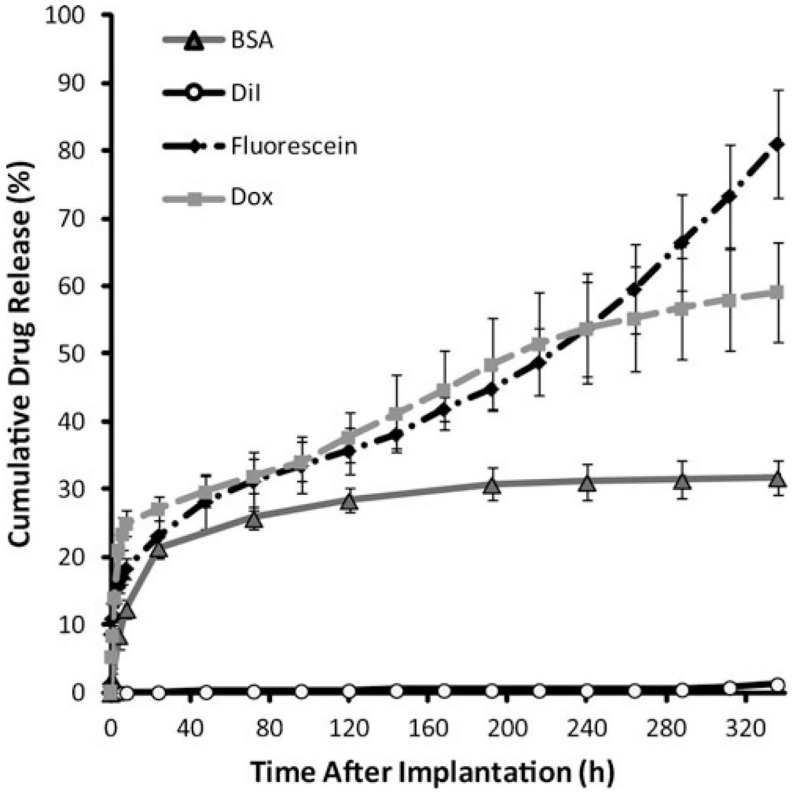

Fig. 2.
Cumulative mass release of drug from the ISFI into PBS (pH 7.4)

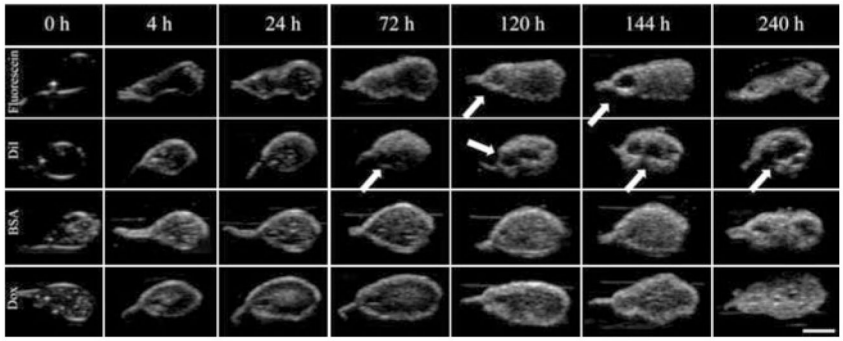

Fig. 3.

Representative gray-scale ultrasound images of implants acquired over a period of 240 h; each *row* is representative of implants loaded with different drugs: Fluorescein, DiI, BSA, and Dox. The *scale bar* represents 2.5 mm. Pore formation is indicated with *arrows*

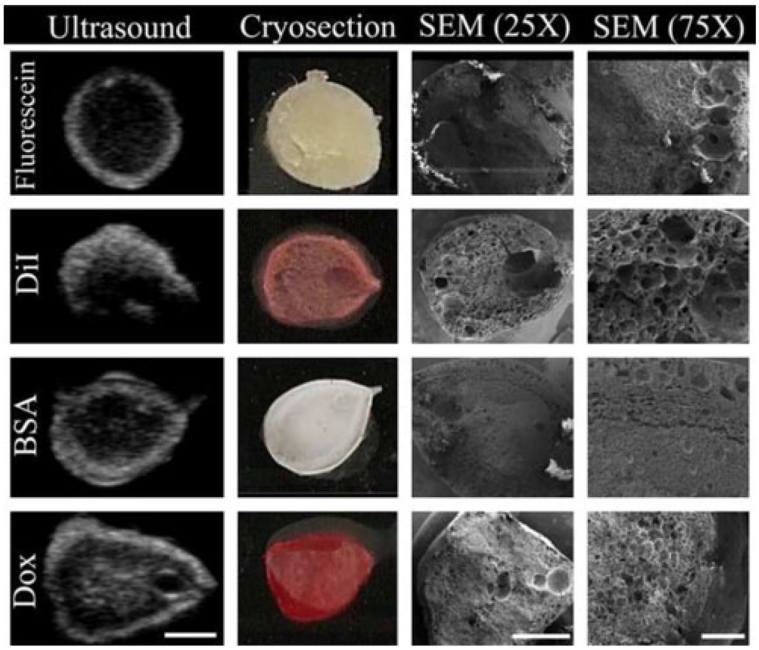

Fig. 4.

Validation of implant morphology ultrasound data. Shown are representative images from ultrasound (Day 3, *scale bar*=2.5 mm), digital camera, SEM (×25 magnification, *scale bar*=2 mm), and higher magnification SEM (×75 magnification, *scale bar*=500 μm)

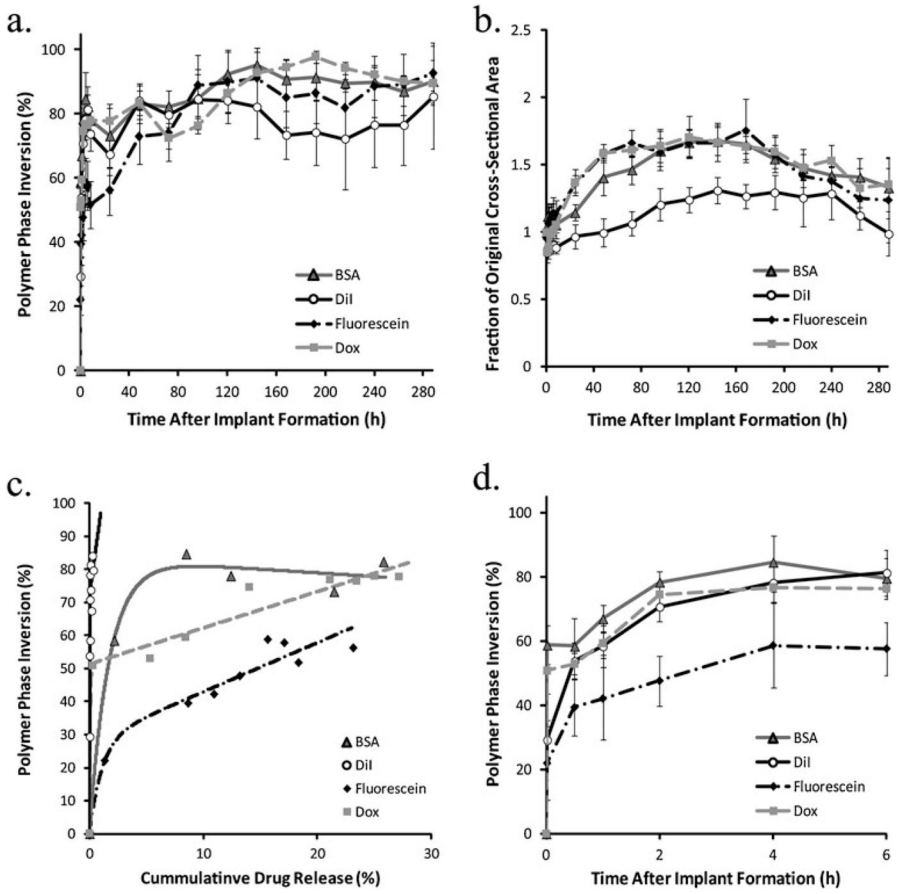

Fig. 5.

a Quantitative formation data acquired in the same implants over the course of 12 days. **b** Corresponding quantitative swelling data. **c** Correlation of phase inversion and drug release. **d** Changes in mean gray-scale value over time

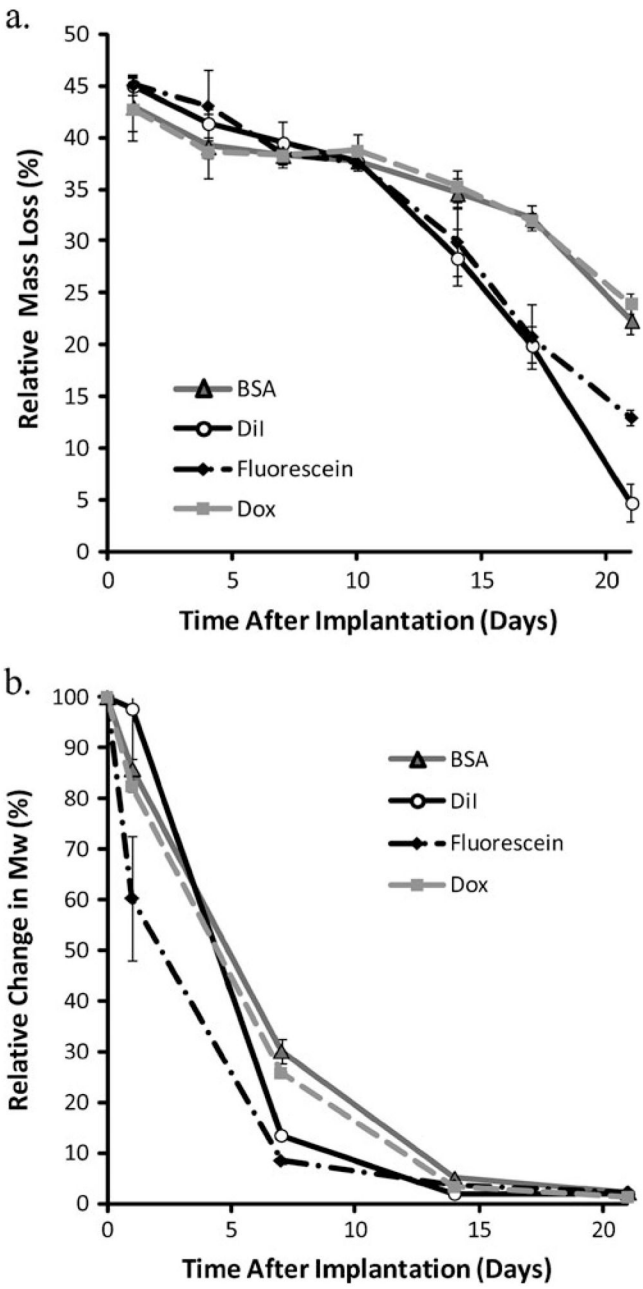

Fig. 6.

a Cumulative erosion data, measured as percent mass loss over time from ISFI formed in PBS (pH 7.4). **b** Degradation analysis measured as change in the weight average Mw over time, with data normalized by the Mw of the polymer before exposure to PBS

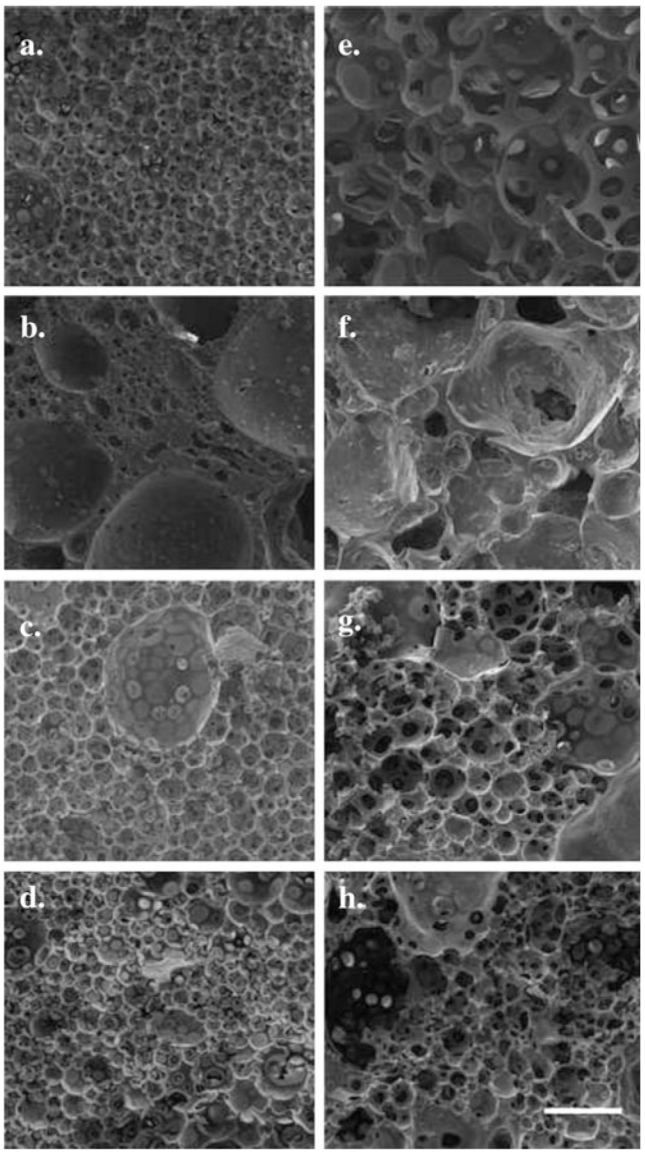

Fig. 7.
SEM images of implants in the bath solution for 3 (**a**–**d**) and 7 days (**e**–**h**) at a magnification of ×250. Each *row* is representative of implants loaded with different drugs: (**a**, **e**) Fluorescein, (**b**, **f**) DiI, (**c**, **g**) BSA, (**d**, **h**) Dox. *Scale bar* represents 100 μm

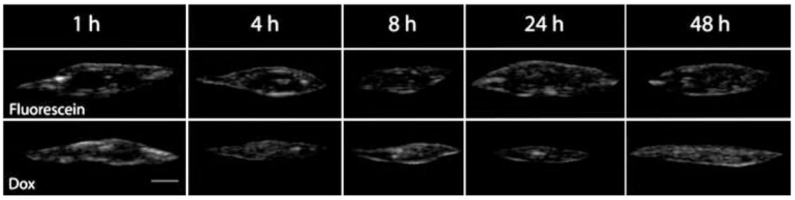

Fig. 8.
Representative ultrasound gray-scale images of implants formed subcutaneously; *scale bar* represents 2.5 mm

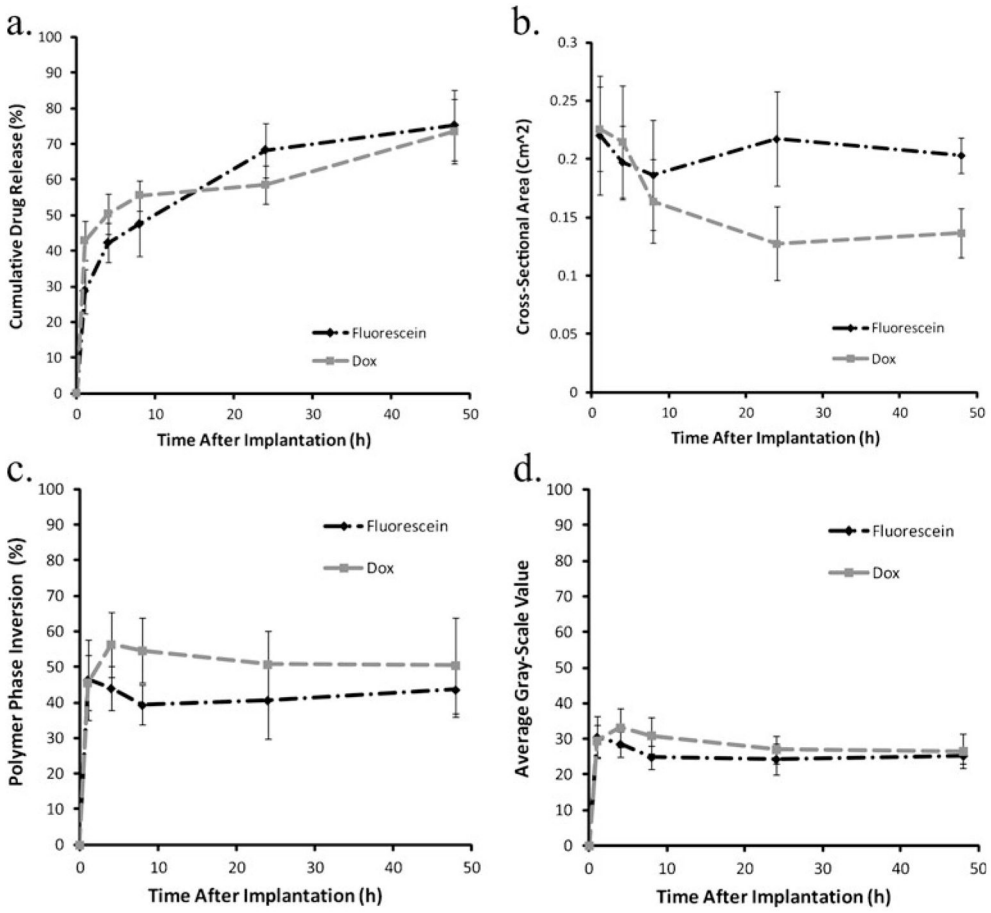

Fig. 9.

a Cumulative mass release of drug from implants injected subcutaneously under the dorsal skin flap of Sprague-Dawley rats over the course of 48 h. **b** Quantitative swelling data for the same implants. **c** Quantitative formation data for implants formed subcutaneously. **d** Changes in mean gray-scale data over time

Table 1

Properties of the drugs used

Properties	Fluorescein	Dox	DiI	BSA
Mw (Da)	376	580	934	66,430
p*Ka*/p*I*	6.4 [44]	7.6–8.4 [2, 42, 43]	N/A	4.7–4.9 [40]

Table 2

Mean release per phase of release

Release	Fluorescein	Dox	DiI	BSA
Burst (%)	23.2±3.3	27.2±1.8	0.2±0.04	21.4±1.5
Diffusion ($\frac{\%}{d}$)	2.7±1.2	3.2±1.1	0.03±0.02	1.0±0.3
Degradation ($\frac{\%}{d}$)	6.5±0.8	1.5±0.3	0.2±0.1	0.2±0.1

Table 3

Correlation coefficients and values obtained from mathematical fit of phase inversion and drug release

Variables	Fluorescein	Dox	DiI	BSA	Dox *in vivo*	Fluorescein *in vivo*
S_0	28.1	51.3	72.0	83.4	48.4	46.2
τ	0.9	14.9	51.6	0.6	1.0	3.4
m	1.5	1.1	25.1	−0.2	0.1	−0.1
R^2	0.97	0.98	0.56	0.99	0.97	0.98